Tiltrotor Descent Aerodynamics: A Small-Scale Experimental Investigation of Vortex Ring State

Mark D. Betzina, Aerospace Engineer
mbetzina@mail.arc.nasa.gov
NASA Ames Research Center
Moffett Field, California

Abstract

An experimental investigation was completed in the NASA Ames 80- by 120-Foot Wind Tunnel with the objective of studying the aerodynamic characteristics of a tiltrotor at high descent angles in helicopter mode. A specific objective was to determine whether tiltrotors behave differently from helicopter rotors when operating in the Vortex Ring State (VRS). A single, 4-foot diameter, 3-bladed rotor, with twist and solidity similar to that of rotors on current tiltrotor aircraft, was tested with an image plane to simulate the mean effect of a second rotor. Rotor performance data were obtained over a wide range of simulated descent conditions, both with and without a semispan wing. Results of this study are presented, including changes in both mean and oscillatory rotor thrust, which are reasonably consistent with helicopter rotor VRS characteristics. Large reductions in mean rotor thrust were found in VRS. These were associated with high levels of low-frequency rotor thrust fluctuations. The image plane had a significant effect on the results, while the wing had a relatively small effect. Implications of these results for the safe operation of tiltrotor aircraft are discussed.

Notation

C_P	Power Coefficient = Torque Coefficient, $Q / \rho(\Omega R)^2 \pi R^3$
C_T	Thrust coefficient, $T / \rho(\Omega R)^2 \pi R^2$
C_{To}	Thrust coefficient in hover
Q	Rotor torque, ft-lb
R	Rotor radius, ft
T	Rotor thrust, lb
V	Air velocity, ft/sec
v_h	Equivalent hover induced velocity, $(T / 2\rho\pi R^2)^{1/2}$, ft/sec
V_{tip}	Rotor tip speed, ΩR, ft/sec
V_x	Freestream velocity component parallel to the rotor tip-path-plane, $V \cos \alpha$, ft/sec
V_z	Freestream velocity component perpendicular to the rotor tip-path-plane, $-V \sin \alpha$, ft/sec, positive in climb
α	Rotor tip-path-plane angle-of-attack, deg, positive in descent (approximately equal to descent angle)
θ	Rotor collective pitch angle at 0.75R, deg
ρ	Air density, slugs/ft^3
σ	Standard deviation from the mean rotor thrust, lb
Ω	Rotor rotational speed, rad/sec
VRS	Vortex Ring State

Introduction

Vortex Ring State (VRS) has been a known phenomenon of rotors in vertical descent or at high descent angles for many years. It occurs when the descent velocity approaches the induced rotor wake velocity, creating recirculation through the rotor disk, and is characterized by rotor thrust loss and thrust oscillations. Loss of rotor thrust and large thrust fluctuations were shown for propellers at very high descent angles in Ref. 1 nearly 40 years ago. Researchers documented large thrust fluctuations in VRS on both single and tandem helicopter rotors in Refs. 2 and 3, respectively. Results for the tandem rotor were very similar to the single rotor except that the tandem rotor did not show the distinct periodicity of thrust fluctuation observed for the single rotor. Other researchers have shown variations in tail rotor thrust as the freestream flow angle varies (Ref. 4). Helicopter pilots typically avoid VRS by limiting descent rate at low forward speeds.

VRS was identified as a possible cause of a recent crash of a V-22 tiltrotor aircraft that was rapidly descending at a rate well beyond the approved flight envelope. This event caused renewed interest in VRS, and raised the question of whether tiltrotor aircraft behaved differently in VRS from single-rotor or tandem helicopters. It was believed that the unique aspects of tiltrotor aircraft, including higher disk loading, higher blade twist, and interactions between the two rotor wakes and the wing, could be responsible for

---

Presented at the American Helicopter Society 57th Annual Forum, Washington, DC, May 9-11, 2001.

different VRS characteristics. However, there was no prior VRS research on tiltrotors to confirm this and no experimental data were available.

An experimental investigation was recently completed in the NASA Ames 80- by 120-Foot Wind Tunnel with the objective of studying the aerodynamic characteristics of a tiltrotor at high descent angles in helicopter mode. A specific objective was to define the region of the flight envelope where VRS occurs and to determine whether tiltrotors behave differently from helicopter rotors when operating in VRS. A single 3-bladed rotor, with high twist and solidity similar to current tiltrotors, was used with an image plane to simulate the mean effect of a second rotor. This paper presents the results of this study.

Test Description

Equipment

Figure 1 shows the test installation in the NASA Ames 80- by 120-Foot Wind Tunnel. The large ratio of wind tunnel size to rotor diameter ensured the absence of wall effects on the rotor wake, even for the very large disturbed flow region associated with VRS. Figure 2 shows the rotor with a semispan wing and image plane installed. The rotor and wing parameters are shown in Table 1.

The 4-ft. diameter wood rotor blades were rigidly mounted to the hub and rotated in the conventional direction for a left-hand tiltrotor, with advancing blade outboard of the wing. The rotor, which did not represent any particular full-scale configuration, is described in more detail in Ref. 5. Relative to the V-22 aircraft, the 4-ft rotor was 10.5% scale, although the twist, planform, chord, and airfoil differed from the V-22. The hub was rigidly mounted to the drive shaft and driven by an electric motor on the inflow side of the rotor. Collective blade pitch was changed manually by rotating the individual blades where they were clamped into the hub. Cyclic pitch was not incorporated. A 5-component rotor balance and an instrumented torque coupling were used to acquire rotor thrust and power.

An image plane was mounted horizontally at the scaled location of the V-22 aircraft centerline. The image plane geometry is shown in Fig. 3. A symmetric airfoil-shaped leading-edge fairing was incorporated as shown to minimize flow separation. The semispan wing approximated a 10.5%-scale model of a V-22 left-hand wing and flap, incorporating the airfoil, sweep, and dihedral of the V-22 aircraft. The wing was mounted at an orientation simulating a 95-deg nacelle angle. The full-span flap was deflected 72.5 deg and the flap gap was open. A nacelle and fuselage were not included. The wing tip was terminated with a horizontal cut at the scaled nacelle centerline location.

Fig. 1. Tiltrotor Descent Aerodynamics test in NASA Ames 80- by 120-Foot Wind Tunnel.

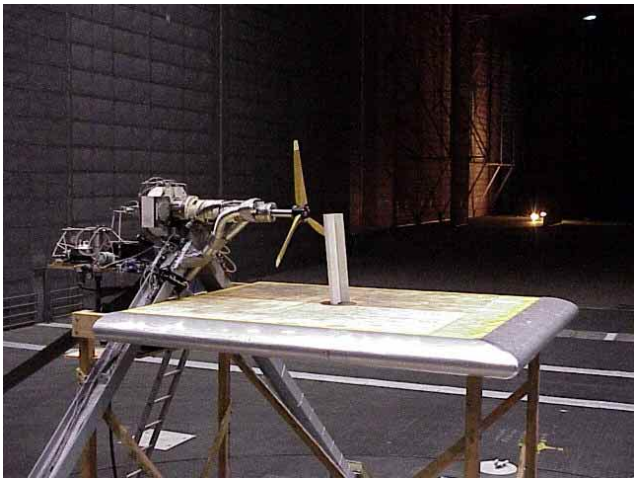

Fig. 2. Rotor with semispan wing and image plane installed.

Table 1. Rotor and wing parameters

Parameter	Value
Rotor radius, R	2.0 ft
Total rotor twist (non-linear)	41 deg
Rotor solidity	0.1194
Wing semispan	2.42 ft
Flap deflection	72.5 deg
Nacelle angle	95 deg

Test Parameters

Rotor performance data were acquired over a range of simulated descent conditions shown in Table 2. Data were obtained at most test conditions both with and without the wing. A limited amount of data was obtained in an isolated rotor configuration with the image plane removed.

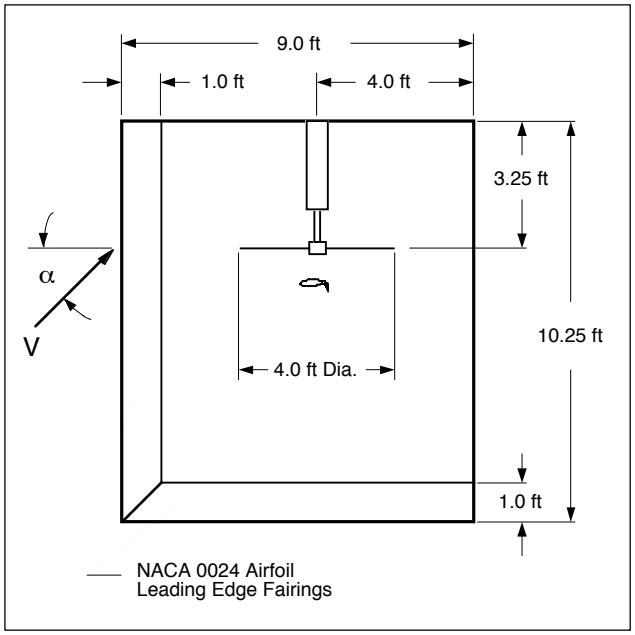

Fig. 3. Image plane geometry.

Table 2. Range of test conditions

Parameter	Value
V_{tip} (ft/sec)	377
V/V_{tip}	0, 0.04, 0.06, 0.08, 0.10, 0.12
θ (deg)	1, 3, 4, 6, 8, 10, 12
α (deg)	0 to 90 (5-deg increments)

The rotor tip speed was held constant at 377 ft/sec throughout the test, significantly lower than full-scale tip speeds. However, by matching full-scale advance ratios (V/V_{tip}) and thrust coefficients (C_T) the velocity ratios between the wake and freestream matched full-scale values. For each combination of advance ratio and collective blade pitch (θ), the tip-path-plane angle-of-attack (α) was varied from 0 deg (edgewise flight) to 90 deg (vertical descent) in 5-deg increments. The simulated aircraft descent angle was considered to be nearly equivalent to α because a tiltrotor aircraft's tip-path-plane at these low airspeeds is typically very close to horizontal, regardless of the descent angle. Therefore, descent angle is used throughout this paper when referring to the tip-path-plane angle-of-attack.

Data Acquisition and Processing

All data were low-pass filtered at 100 Hz (3.33/rev) and sampled at 1024 samples per second for 4 seconds (about 120 revolutions) yielding a time history of 4096 samples for each data point that were averaged to provide mean data. Mean thrust and torque were used to compute thrust and power coefficients, respectively.

Thrust time histories were windowed using a Hanning function. A Fast Fourier Transform (FFT) was performed on the windowed data to obtain a rotor thrust spectrum for each data point. These showed very high magnitudes at the 3/rev and 6/rev harmonics due to the rigid mounting of the rotor blades and hub, and smaller peaks at the other harmonics from 1/rev to 5/rev. Therefore, filtered rotor thrust time histories were obtained by removing all frequency content above 20 Hz (0.67/rev) and then reconstructing the time history as follows. An FFT was performed on the original acquired time history without windowing. Then all coefficients for frequencies above 20 Hz were zeroed. An inverse FFT was performed to yield a filtered time history. Standard deviation from the mean was computed for each of these filtered time histories to quantify the magnitude of the thrust fluctuations.

Results and Discussion

The effects of VRS on mean rotor thrust and power and on the oscillatory rotor thrust will be shown for the complete configuration with the semispan wing and image plane installed. Various ways of defining a VRS boundary will be discussed. The effects of the image plane and semispan wing will be shown. Finally, implications of these results for tiltrotor aircraft will be discussed.

Mean Rotor Thrust and Power

Figures 4 and 5 show the variation of thrust and power coefficients as a function of descent angle, for constant advance ratio and collective pitch. Figure 4 indicates that for low descent angles, the thrust increases with descent angle. At angles between 20 deg and 45 deg, depending on the collective pitch and advance ratio, this trend reverses and thrust decreases with increasing descent angle. However, there is very little change in thrust at the lowest advance ratio of 0.04. The descent angle at which the thrust starts to decline is lower for high collectives than for low collectives. The thrust reduction above 20-45 deg is a result of VRS, and is caused by recirculation of the rotor wake. The power, however, remains relatively unchanged through the full range of descent angles, as shown in Fig. 5. Hence the power is primarily determined by the collective pitch angle at which the rotor is operating.

At low descent angles, the slopes of the curves in Fig. 4 increase with higher advance ratio, indicating that increases in thrust with descent angle are greater for higher advance ratios. However, the negative slope at high descent angles, caused by VRS, is highest at an advance ratio of 0.08 (fig. 4c), indicating that the reduction in thrust with increasing descent angle is greatest near this speed. Figure 6 is obtained by cross plotting Fig. 4c to obtain thrust coefficient versus

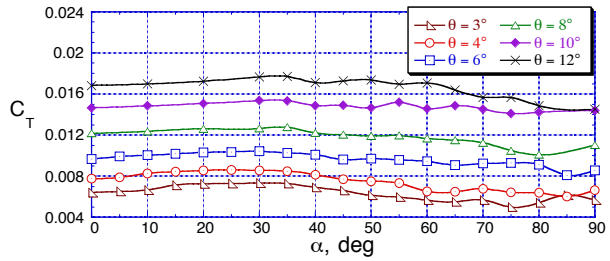

a) V/V_{tip} = 0.04

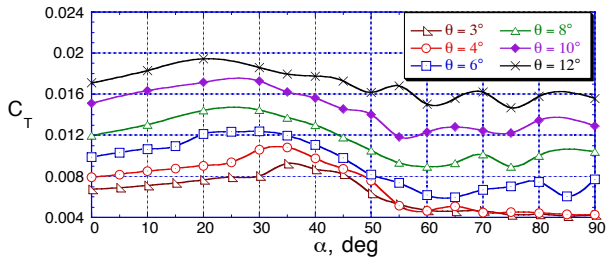

b) V/V_{tip} = 0.06

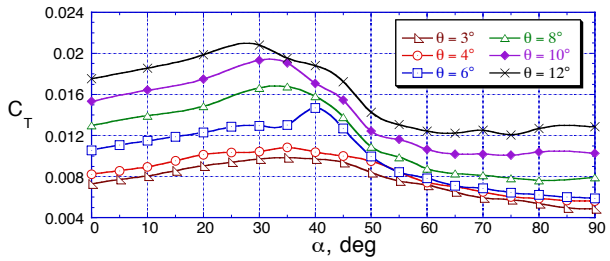

c) V/V_{tip} = 0.08

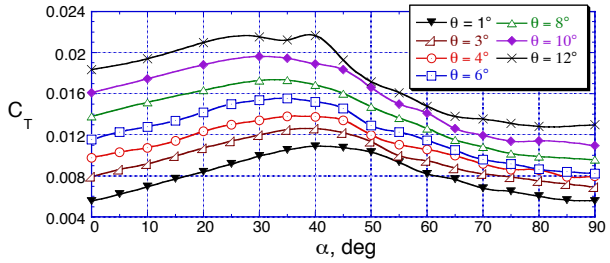

d) V/V_{tip} = 0.10

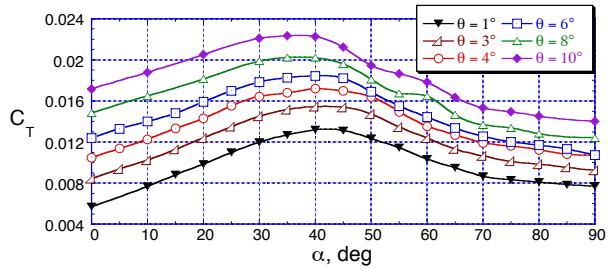

e) V/V_{tip} = 0.12

Fig. 4. Variation of rotor mean thrust with descent angle, semispan wing and image plane installed.

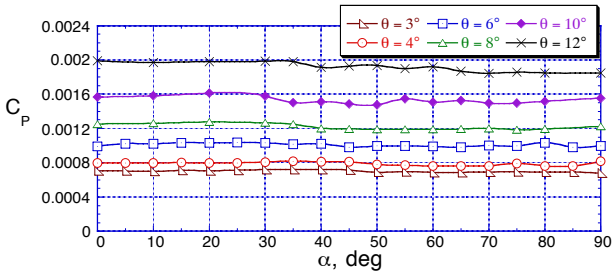

a) V/V_{tip} = 0.04

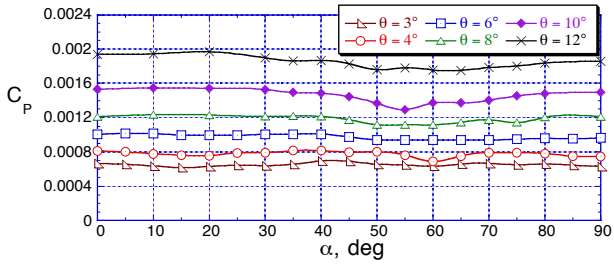

b) V/V_{tip} = 0.06

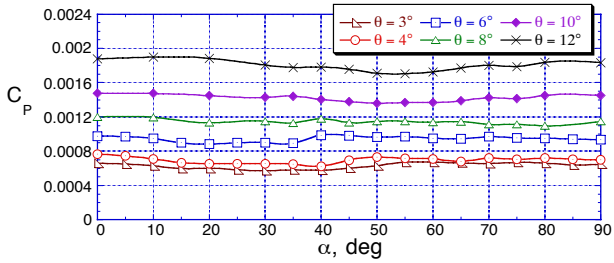

c) V/V_{tip} = 0.08

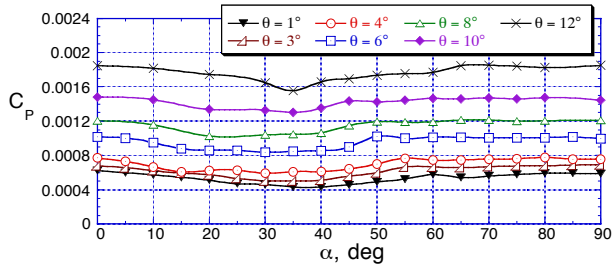

d) V/V_{tip} = 0.10

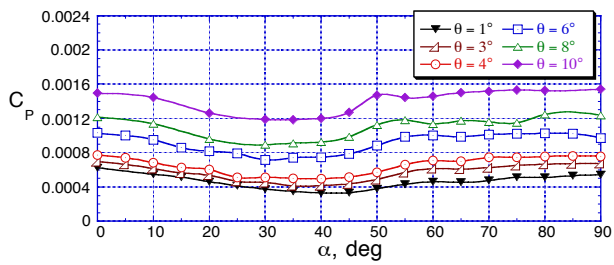

e) V/V_{tip} = 0.12

Fig. 5. Variation of rotor mean power with descent angle, semispan wing and image plane installed.

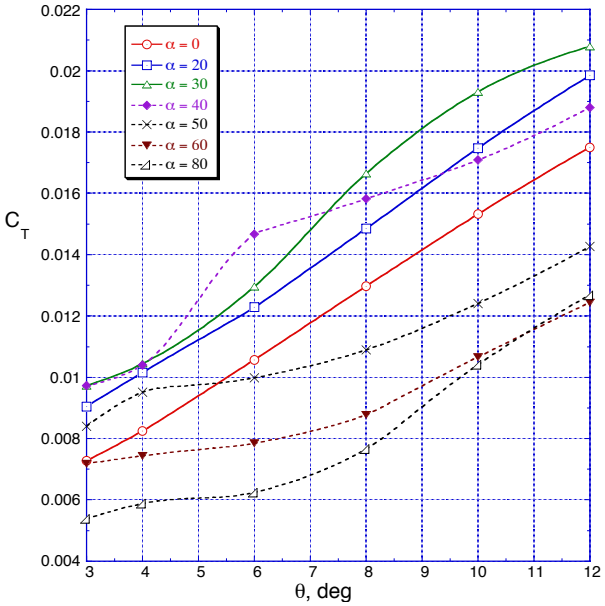

Fig. 6. Variation of rotor thrust with collective pitch, V/V_{tip} = 0.08, semispan wing and image plane installed.

collective pitch for constant descent angles. The slopes of the curves in Fig. 6 are lower at high descent angles than at low descent angles, indicating that VRS causes the rotor's effective lift curve slope to be reduced. The slope change occurs between 30-deg and 40-deg descent angle, which is consistent with where the thrust starts to decline in Fig. 4c. However, the slope is always positive, producing more thrust at higher collective pitch.

Cross plotting from Fig. 6, the collective pitch required to maintain constant rotor thrust for various thrust levels is shown in Fig. 7. The higher thrust curves are incomplete because collectives above 12 deg were not tested. As

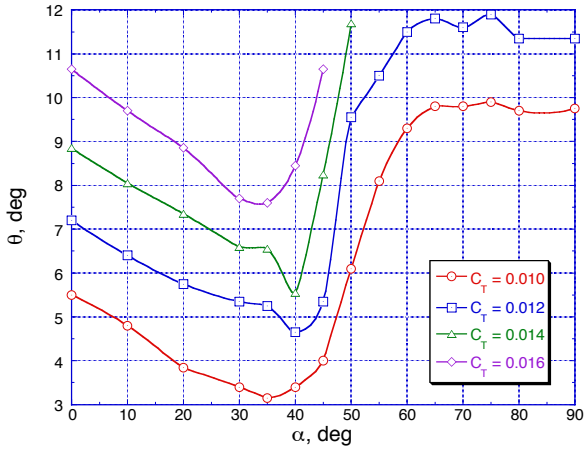

Fig. 7. Collective pitch required to maintain constant rotor thrust, V/V_{tip} = 0.08, semispan wing and image plane installed.

expected, the required collective pitch at low descent angles declines as descent angle increases. However, at descent angles from 40 deg to 60 deg, large increases in collective pitch are required as a result of the thrust reduction and lower effective lift curve slope caused by VRS. Figure 8 shows both the collective pitch and power coefficient required to maintain a constant thrust coefficient of 0.014, indicating that the required power has the same trend as the required collective pitch.

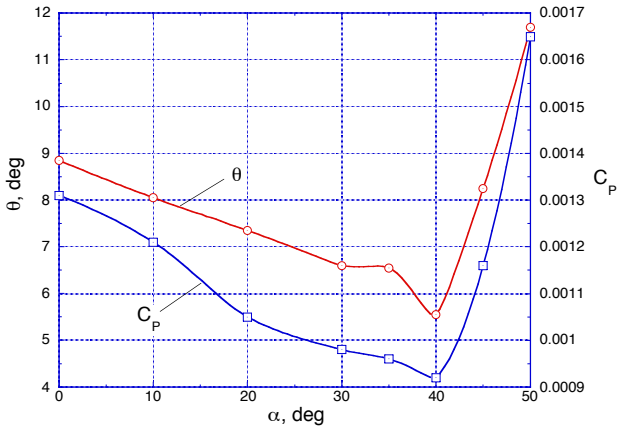

Fig. 8. Collective pitch and power required to maintain constant rotor thrust, C_T = 0.014, V/V_{tip} = 0.08, semispan wing and image plane installed.

Vortex Ring State Boundary

Various methods of defining a VRS boundary were explored. An appropriate boundary should designate the area of the flight envelope where the effects of VRS are apparent. This requires choosing appropriate parameters for displaying the flight conditions as well as defining criteria for VRS effects. A typical way of displaying the flight condition for rotor wake phenomena is to use components of the freestream velocity, V_x and V_z, normalized by the effective hover induced velocity, v_h, producing non-dimensional velocity ratios that depend on thrust, freestream velocity, and descent angle. V_x and V_z are defined as the velocity components that are parallel and perpendicular to the rotor tip-path-plane, respectively. However, for the low-speed cases investigated here where the rotor tip-path-plane is very close to horizontal, V_x and V_z can be considered the horizontal and descent velocities, respectively. Much of the remaining results will be displayed on plots of V_z/v_h versus V_x/v_h.

One method of defining a VRS boundary would use mean thrust reduction as an indicator. The maximum thrust points of Fig. 4, where the thrust starts declining, could be used to indicate the beginning of VRS. These points are shown in Fig. 9 with a curve fit of the data. While these points show a fair amount of scatter, partly because of the 5-deg increments in descent angles tested and partly

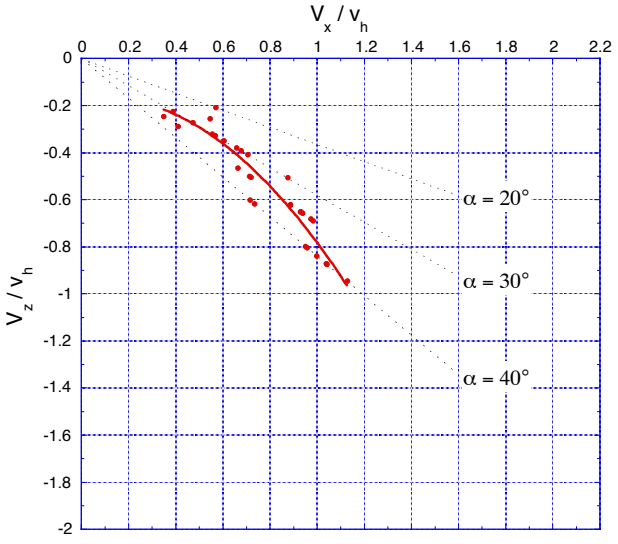

Fig. 9. Vortex Ring State boundary using maximum mean thrust, semispan wing and image plane installed.

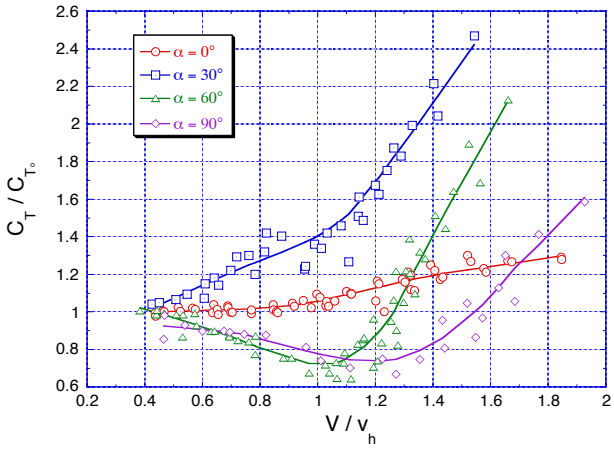

Fig. 10. Variation of normalized rotor thrust with normalized velocity, semispan wing and image plane installed, $C_T > 0.006$.

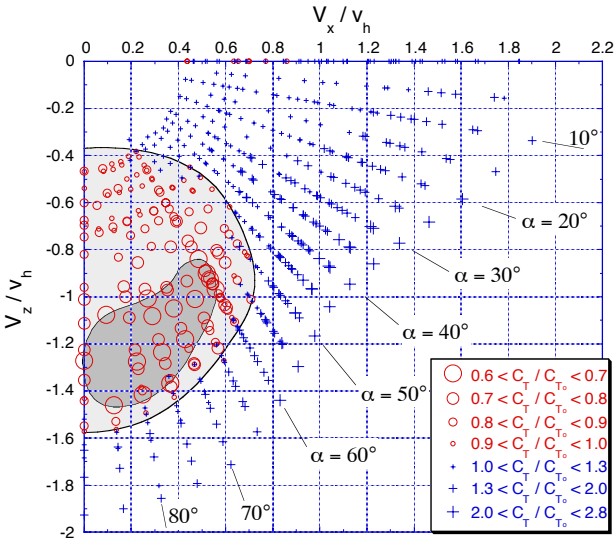

Fig. 11. Rotor mean thrust changes, $C_T > 0.006$, semispan wing and image plane installed.

because of a dependency on advance ratio, they indicate that the VRS boundary is between 20-deg and 40-deg descent angle for horizontal normalized velocity ratios from 0.35 to 1.1.

One way to quantify the magnitude of thrust reduction caused by VRS is to compare the thrust coefficient to a reference value, such as the hover thrust coefficient (C_{To}) measured at the same collective pitch. The thrust ratio (C_T/C_{To}) plotted versus normalized total velocity (V/v_h) is presented in Fig. 10 for several descent angles. Data for all advance ratios and collectives tested are plotted except for points with low thrust levels. Data with thrust coefficients less than 0.006 have been excluded because the measured thrust ratio (C_T/C_{To}) becomes inaccurate as the thrust approaches zero. Note that the data for each descent angle are nearly independent of advance ratio and collective pitch when normalized in this manner. As shown, the greatest thrust reduction occurs between velocity ratios (V/v_h) of 0.8 and 1.2 for 60-deg descent angle and between 1.0 and 1.4 for 90 deg (vertical descent).

A more comprehensive view of these data is obtained in Fig. 11, which displays data acquired at all five advance ratios and all descent angles from 0 deg to 90 deg by plotting normalized vertical descent velocity (V_z/v_h) versus normalized horizontal velocity (V_x/v_h). The plus symbols indicate points where the thrust ratio (C_T/C_{To}) is greater than one, and the circles indicate thrust ratios less than one. The size of the symbol indicates the magnitude of the thrust ratio, with larger symbols associated with ratios further from one. The shaded area encompasses thrust ratios less than one, with the darker shading designating the lowest thrust ratios. Again, low thrust data with thrust coefficients less than 0.006 have been excluded. A definite pattern is apparent, with the lowest thrust ratios in a region centered at about $\alpha = 75$ deg and $V_x/v_h = 0.3$. This indicates the region where the thrust reduction due to VRS is greatest, which appears to extend from 60-deg to 90-deg descent angle. The boundary of the lightly shaded region, designating the boundary of thrust ratios less than one, is reasonably well defined. The upper portion of this boundary is located at descent angles between 45 deg and 55 deg for V_x/v_h between 0.3 and 0.7. While this boundary is somewhat arbitrary, it may define a contour line where the severity of VRS, based on mean thrust reduction, is approximately equal. This boundary is at higher descent angles than the boundary in Fig. 9 because the thrust must decline substantially below the maximum thrust used in Fig. 9 to reach a thrust ratio of one at the hover thrust value.

Oscillatory Rotor Thrust

Other researchers (Ref. 2) have used the amplitude of thrust fluctuations, based on the difference between maximum and minimum measured thrust, to define the region where VRS occurs for helicopter rotors. The parameter used to quantify thrust fluctuations for this paper is three standard deviations (3σ) of the filtered rotor thrust time history normalized by the mean rotor thrust. It is believed that this parameter is comparable to, but more consistent than, the difference between maximum and minimum measured thrust and is less dependent on the sample time.

The oscillatory rotor thrust magnitudes are shown in Fig. 12, for each of the five advance ratios tested, on plots of normalized vertical descent velocity (V_z/v_h) versus normalized horizontal velocity (V_x/v_h). Low thrust data with thrust coefficients less than 0.006 have been excluded. The lowest fluctuations occur at descent angles less than 30 deg. The highest oscillatory magnitudes, between 30% and 52% of the mean rotor thrust, were obtained at an advance ratio of 0.06 for descent angles between 50 deg and 80 deg

All of the data in Fig. 12, plus some additional points at intermediate advance ratios, are displayed on one plot in Fig. 13. Although there appears to be some dependency on advance ratio, this plot provides a reasonably consistent picture of the region where significant thrust fluctuations occur. The extent of this region is similar to the region of reduced thrust shown in Fig. 11. However, the region of highest thrust fluctuation (> 30%), designated by the shaded area in Fig. 13, is at lower descent angles and lower descent velocities than the region with the greatest thrust reduction identified in Fig. 11. This region of high thrust fluctuation is centered at a descent angle of 65 deg and a normalized horizontal velocity (V_x/v_h) of 0.37. This region, as well as the magnitude of fluctuation, is remarkably consistent with the region identified in Ref. 2 for a helicopter rotor. This leads one to believe that even with a wing and image plane, tiltrotors with twist and solidity much higher than helicopter rotors may behave almost the same as helicopter rotors in VRS. However, as shown below, the isolated rotor data are quite different, implying that the wing and image plane effects may fortuitously compensate for the differences caused by high twist and solidity. An experiment utilizing the same test setup with different rotors may be necessary to conclusively resolve this question.

The highest oscillatory thrust (51.9%) was obtained at V/V_{tip} = 0.06, α = 60 deg and θ = 12 deg. The filtered rotor thrust time history for this condition is shown in Fig. 14 along with time histories for other collective pitch angles. The rotor thrust spectra for these conditions are shown in Fig. 15. All of these cases indicate a dominant frequency of 0.25 Hz. However, because this is the minimum frequency obtainable from a 4-second data sample, the accuracy of the dominant frequency is

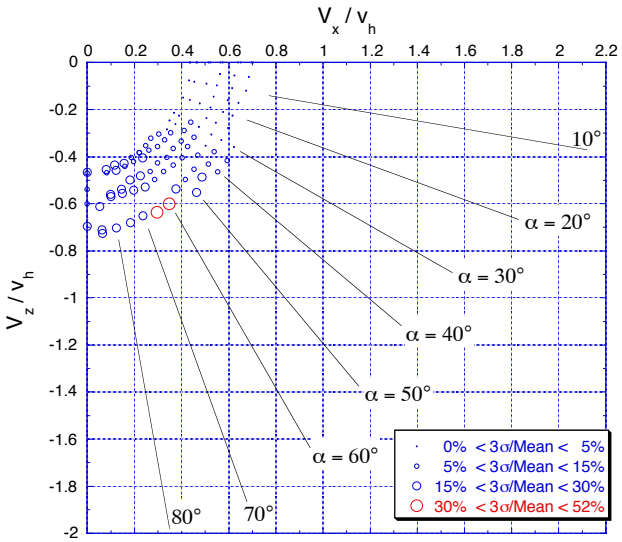

Fig. 12a) V/V_{tip} = 0.04

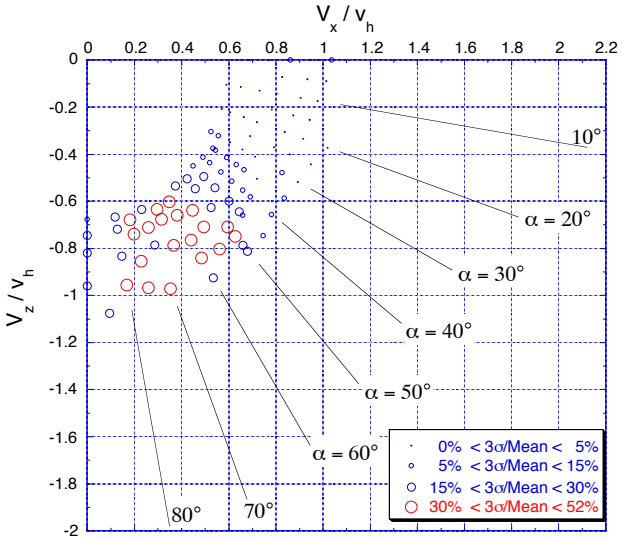

Fig. 12b) V/V_{tip} = 0.06

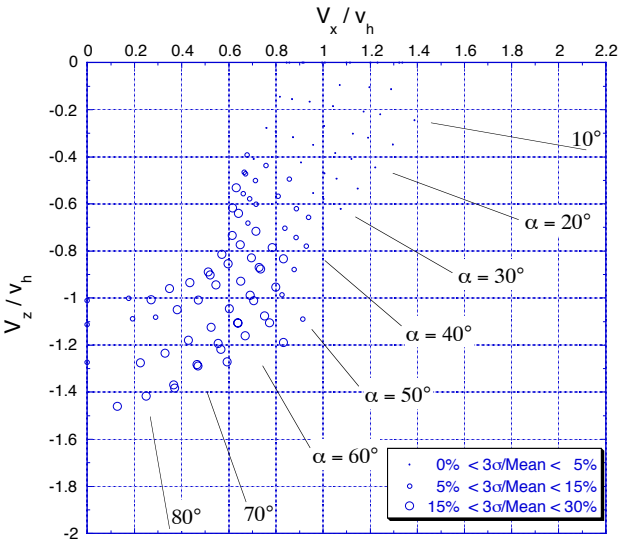

Fig. 12c) V/V_{tip} = 0.08

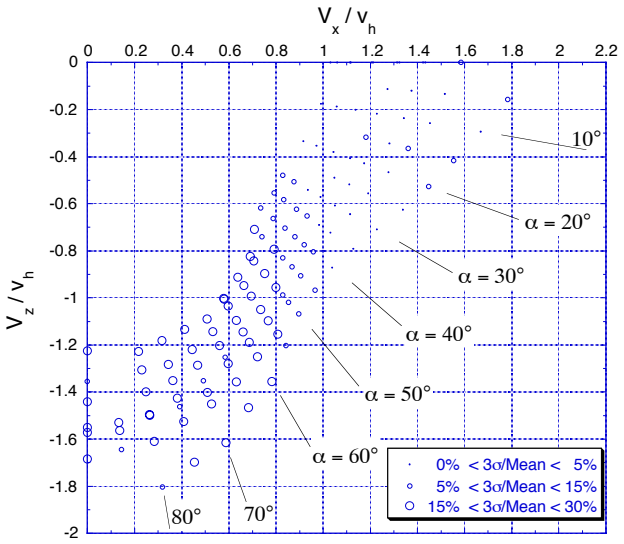

Fig. 12d) V/V_{tip} = 0.10

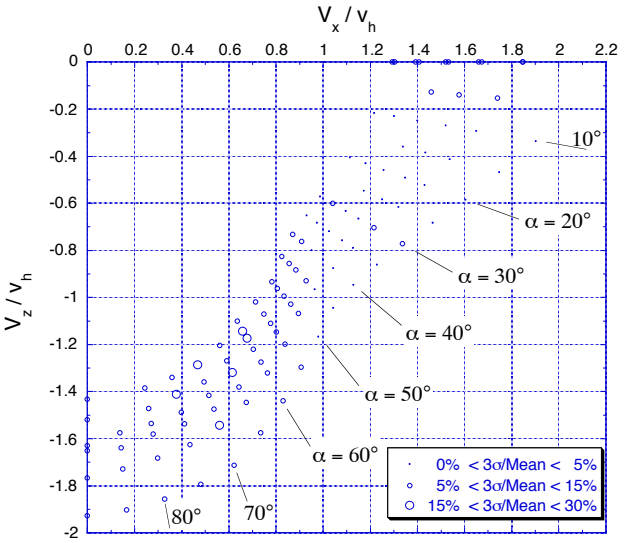

Fig. 12e) V/V_{tip} = 0.12

Fig. 12. Oscillatory rotor thrust magnitudes for constant advance ratio, $C_T > 0.006$, semispan wing and image plane installed.

questionable. Nonetheless, it appears that there is a consistent thrust fluctuation frequency with a period near 4 seconds. It is not known how this frequency would scale up to a full-scale rotor. If it is assumed that the frequency is directly proportional to velocity and inversely proportional to length, then it could have a period of about 18 seconds for a 38-foot diameter tiltrotor at full-scale tip speed.

The effect of descent angle on the oscillatory thrust magnitude for constant collective pitch is shown in Fig. 16 for the same advance ratio of 0.06. The thrust fluctuations start increasing at 20 deg and continue to grow with descent angle up to 60 deg or 70 deg and then decline as

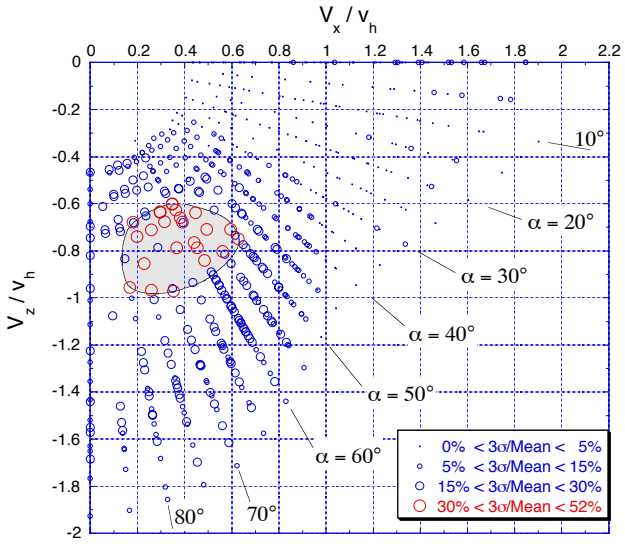

Fig. 13. Oscillatory rotor thrust magnitudes, $C_T > 0.006$, semispan wing and image plane installed.

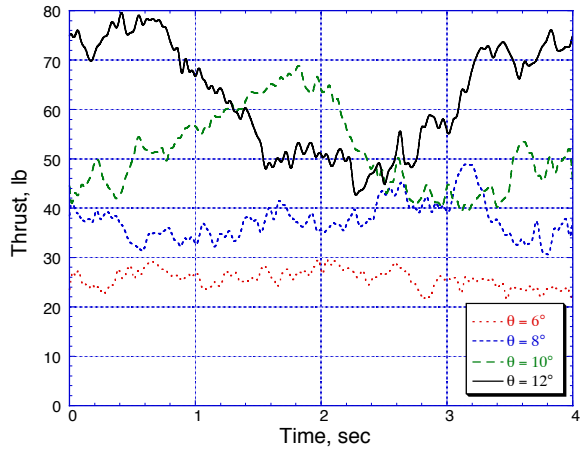

Fig. 14. Filtered rotor thrust time history, V/V_{tip} = 0.06, α = 60 deg, semispan wing and image plane installed.

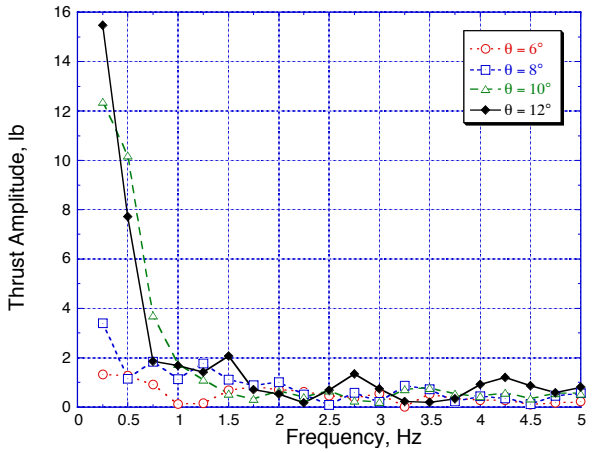

Fig. 15. Rotor thrust spectrum, V/V_{tip} = 0.06, α = 60 deg, semispan wing and image plane installed.

descent angle is increased to 90 deg. Figure 17 shows the effect of descent angle for different advance ratios at a constant collective pitch of 10 deg. Although the trend is similar for advance ratios other than 0.06, the oscillatory thrust is significantly lower.

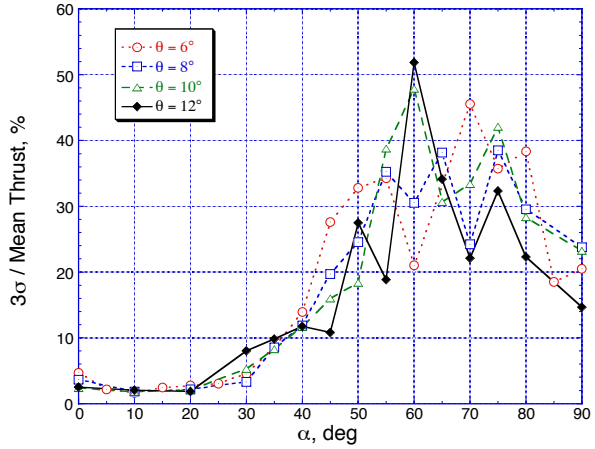

Fig. 16. Effect of descent angle on oscillatory rotor thrust magnitude, V/V_{tip} = 0.06, semispan wing and image plane installed.

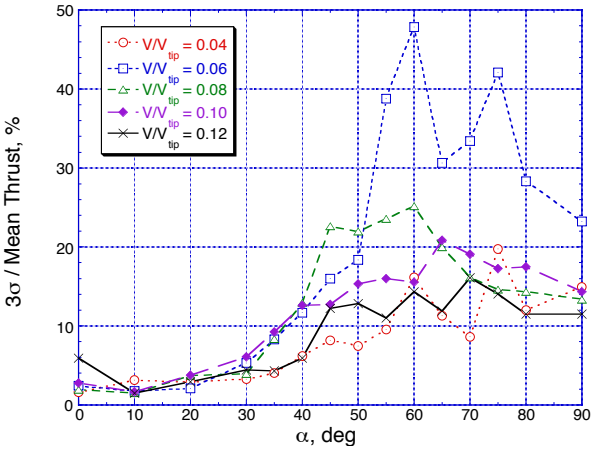

Fig. 17. Effect of descent angle on oscillatory rotor thrust magnitude, θ = 10 deg, semispan wing and image plane installed.

Image Plane and Semispan Wing Effects

Isolated rotor data were acquired at θ = 6 deg and θ = 10 deg. The effects of the image plane and semispan wing on the mean rotor thrust characteristics are shown in Fig. 18 for θ = 10 deg. The isolated rotor shows much less thrust variation with descent angle for advance ratios of 0.06 and 0.08 indicating that the effects of VRS may be less severe for an isolated rotor. At the higher advance ratios of 0.10 and 0.12, the isolated rotor thrust does not decline substantially until the descent angle reaches 80 deg. The wing appears to have only a small effect on the mean rotor thrust, causing small increases in thrust at low to moderate descent angles. The results for θ = 6 deg are similar.

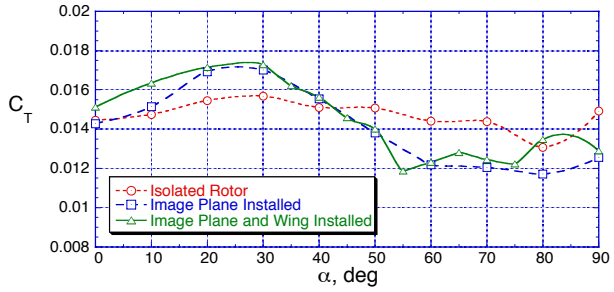

a) V/V_{tip} = 0.06

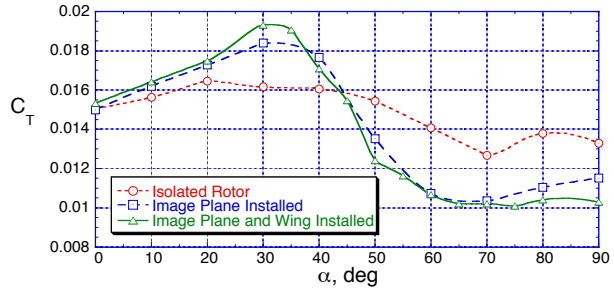

b) V/V_{tip} = 0.08

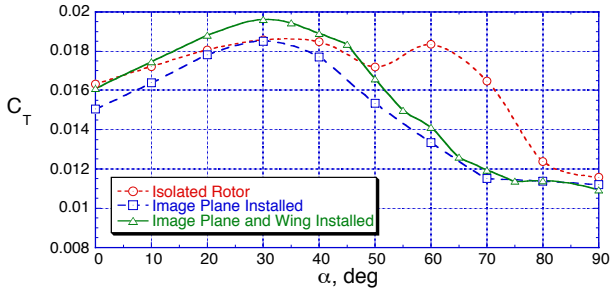

c) V/V_{tip} = 0.10

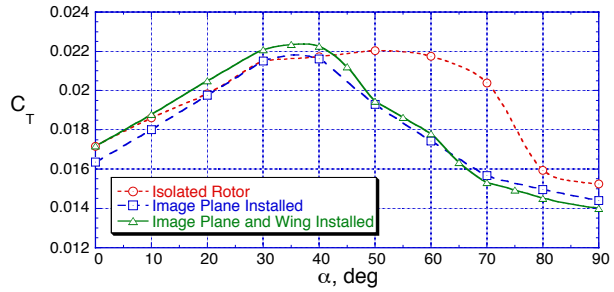

d) V/V_{tip} = 0.12

Fig. 18. Effect of image plane and semispan wing on rotor mean thrust, θ = 10 deg.

Figures 19 and 20 show the mean rotor thrust changes for all test conditions acquired with the isolated rotor configuration and for the image plane configuration with the wing off, respectively. Figure 11 shows similar data for the configuration with both the wing and image plane installed. Again, low thrust data with thrust coefficients less than 0.006 are excluded. Figure 19 confirms that the isolated rotor generally has smaller mean thrust reductions and smaller thrust increases over most of the test range compared to the image plane configuration. Comparing Fig. 20 with Fig. 11 indicates that the wing appears to have very little effect.

Figures 21 and 22 show the oscillatory rotor thrust magnitudes for the isolated rotor configuration and for the image plane configuration with the wing off, respectively. Figure 13 shows similar data for the configuration with both the wing and image plane installed. The isolated rotor has lower thrust fluctuations at descent angles from 30 deg to 50 deg, but significantly higher thrust fluctuations, up to 91%, for the higher normalized speeds at α = 80 deg and α = 90 deg. Comparing Fig. 22 with Fig. 13, it appears that the wing has a relatively small effect on thrust fluctuations.

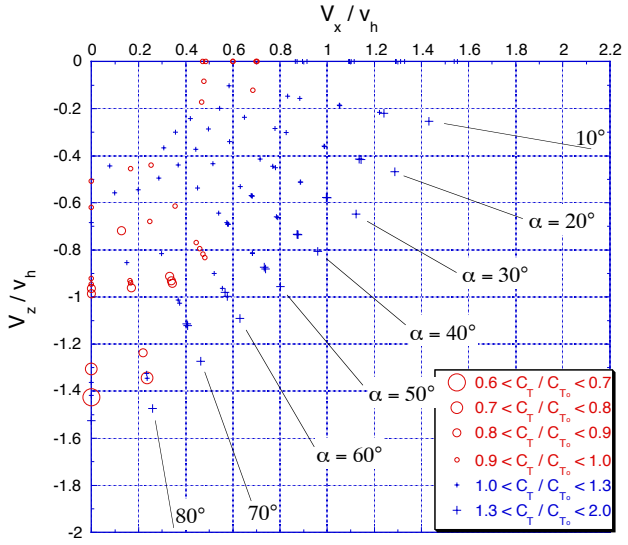

Fig. 19. Isolated rotor mean thrust changes, $C_T > 0.006$

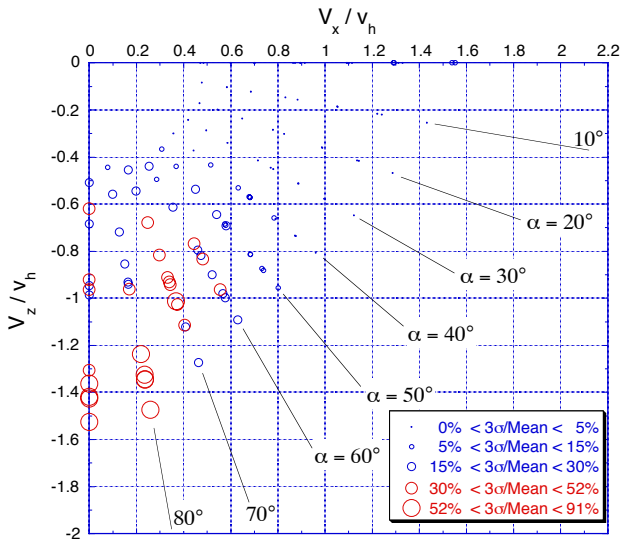

Fig. 21. Isolated rotor oscillatory thrust magnitudes, $C_T > 0.006$.

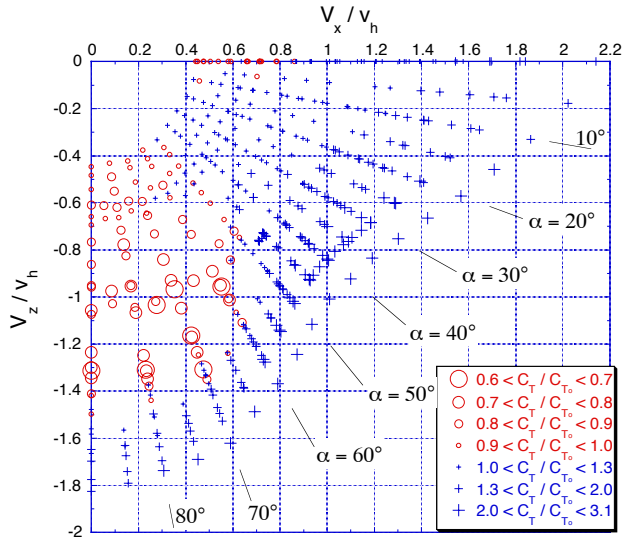

Fig. 20. Rotor mean thrust changes, $C_T > 0.006$, wing off, image plane installed.

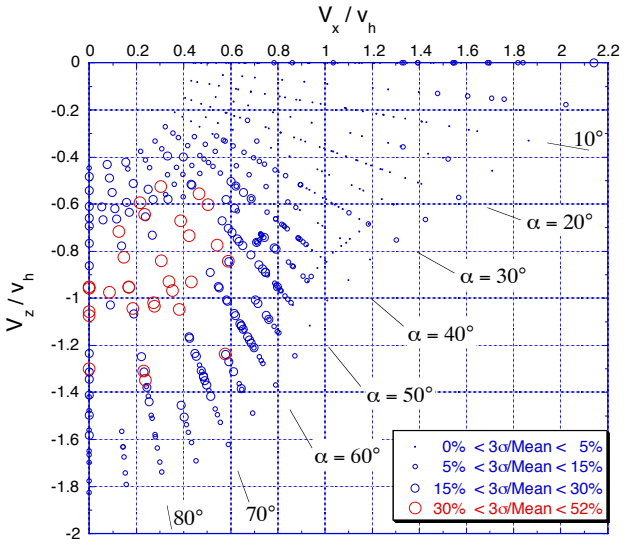

Fig. 22. Oscillatory rotor thrust magnitudes, $C_T > 0.006$, wing off, image plane installed.

One of the highest oscillatory thrust cases for the isolated rotor occurred at an advance ratio of 0.08, descent angle of 80 deg, and θ = 6 deg. The trend of the oscillatory thrust magnitude with descent angle for this condition is shown in Fig. 23. The thrust fluctuations start increasing at 30 deg and reach a maximum at 80 deg that is much higher than the image plane configurations. Figure 24 indicates that the dominant frequency of this large fluctuation is at 0.5 Hz. The image plane configurations also show peaks near 0.5 Hz although not nearly as dominant. It appears that the presence of the image plane may help to stabilize the flow, reducing the oscillatory thrust magnitude. However, this may not be representative of a two-rotor configuration where two unsteady rotor wakes are interacting with each other. It is anticipated that a two-rotor configuration could have greater thrust fluctuations than the isolated rotor.

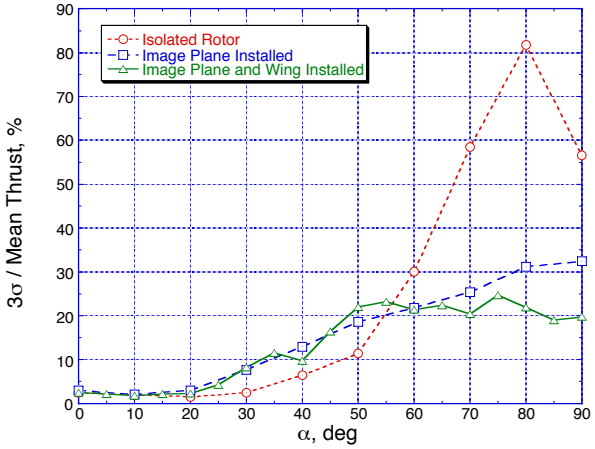

Fig. 23. Effect of image plane and semispan wing on oscillatory rotor thrust magnitude, V/V_{tip} = 0.08, θ = 6 deg.

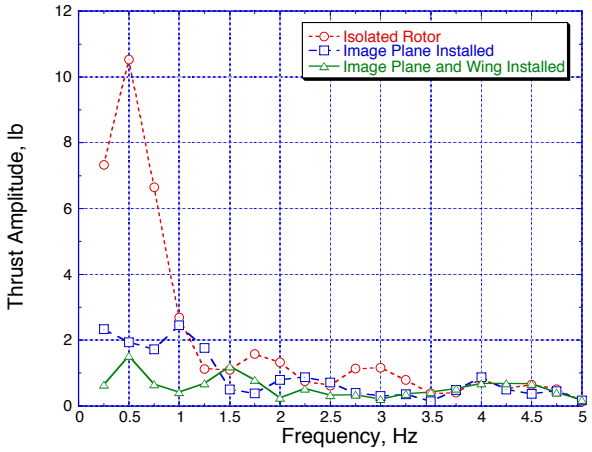

Fig. 24. Effect of image plane and semispan wing on rotor thrust spectrum, V/V_{tip} = 0.08, θ = 6 deg, α = 80 deg.

Figure 25 shows the effects of the image plane and wing on the rotor thrust spectrum for a case at 60-deg descent angle where the image plane and wing configuration showed high oscillatory thrust. All three configurations have similar spectra with the dominant frequency at 0.25 Hz.

The image plane may not accurately represent the mean effect of another rotor and it is certainly not simulating the unsteady effects of two interacting rotor wakes. However, the fact that the image plane has a large effect indicates that a second rotor would be likely to cause significant, although possibly different, effects. Therefore, the two-rotor configuration may be an important factor in determining VRS characteristics for tiltrotor aircraft. Further research should be conducted with two rotors.

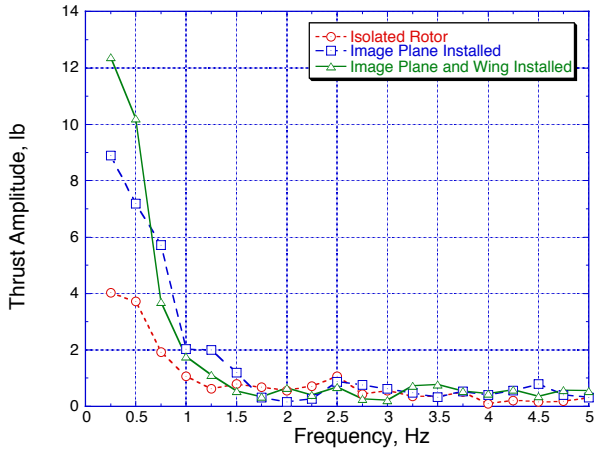

Fig. 25. Effect of image plane and semispan wing on rotor thrust spectrum, V/V_{tip} = 0.06, θ = 10 deg, α = 60 deg.

Implications for Tiltrotor Aircraft

As discussed above, the unique configuration of two side-by-side rotors inherent in tiltrotor aircraft may be an important factor in determining specific VRS characteristics. In addition, even though the oscillatory rotor thrust magnitudes may be similar to helicopter rotors, thrust fluctuations could have implications for roll control of a tiltrotor aircraft. Any differential thrust between the left and right rotor will cause a roll moment that must be counteracted by differential collective pitch in order to maintain a wings-level attitude. This is typically accomplished by an automated flight control system in current tiltrotor aircraft. As discussed above, the period of the rotor thrust fluctuations could be very long, about 18 seconds. Assuming that the thrust fluctuation of each rotor is independent and not in phase with each other, this could lead to significant roll moment oscillations with a similarly long period. An automatic flight control system responding to this low-frequency roll

oscillation could use a significant amount of its differential collective authority.

It is not clear whether the image plane utilized in this test provides correct results for a two-rotor configuration. However, if tiltrotor aircraft characteristics are similar to those shown in Fig. 4, the slope changes that occur when entering VRS could affect the aircraft's response to the flight controls. An automated control system designed to anticipate these characteristics could possibly assist the pilot in VRS.

It is difficult to infer the significance of VRS effects on a tiltrotor aircraft from the data obtained in this test. Further wind tunnel testing is needed with a two-rotor configuration, including the effects of sideslip, to determine the aerodynamic characteristics of tiltrotor aircraft in VRS. Once this information is available, rigorous six-degree-of-freedom simulations and flight testing should be conducted to fully document VRS effects on tiltrotor aircraft.

Conclusions

Vortex Ring State (VRS) has serious implications for tiltrotor aircraft, just as it does for helicopters. However, the unique configuration of two side-by-side rotors may cause significant differences from helicopters in the way the aircraft responds to VRS. But tiltrotor aircraft also have the unique capability of rapidly tilting the nacelles forward, which can be used to quickly move out of a VRS flight condition. VRS occurs at descent angles well beyond typical flight paths, and can be easily avoided by limiting descent rate at low forward speed. However, further research on VRS for tiltrotor aircraft should be conducted to better understand the flight characteristics and perhaps develop ways to mitigate VRS effects.

Specific findings and recommendations from the research reported in this paper are:

1. VRS effects begin between 20-deg and 40-deg descent angle, depending on rotor thrust and freestream velocity. No effects were found at descent angles less than 20 deg.

2. VRS causes mean rotor thrust reductions, thrust fluctuations, and an effective reduction in the rotor's lift curve slope.

3. Maximum rotor thrust fluctuations in VRS (quantified by three standard deviations) were 52% of the mean thrust for the image plane configuration and 91% for the isolated rotor configuration.

4. Rotor thrust fluctuations appeared to have a characteristic period of 2 to 4 seconds for the model rotor tested. This could be as long as 9 to 18 seconds for a full-scale tiltrotor aircraft. Further research is required to determine how this frequency varies with scale and velocity.

5. The image plane had a significant effect on the results, implying that a two-rotor configuration may have significantly different VRS characteristics than a single rotor. Further research is necessary to determine VRS characteristics for a two-rotor configuration.

6. The semispan wing had a relatively small effect on VRS characteristics.

7. VRS may cause very low frequency roll oscillations in a tiltrotor aircraft.

8. Further research is required, including wind tunnel tests, rigorous simulations, and flight testing to fully understand the effects of VRS on tiltrotor aircraft.

References

1. Yaggy, P. and Mort, K., "Wind-Tunnel Tests of Two VTOL Propellers in Descent," NASA TN D-1766, March 1963.

2. Washizu, K., Azuma, A., Koo, J., and Oka, T., "Experiments on a Model Helicopter Rotor Operating in the Vortex Ring State," Journal of Aircraft, Vol. 3, No. 3, May-June 1966.

3. Washizu, K., Azuma, A., Koo, J., and Oka, T., "Experimental Study on the Unsteady Aerodynamics of a Tandem Rotor Operating in the Vortex Ring State," American Helicopter Society 22nd Annual Forum, Washington, D.C., May 1966

4. Empey, R. W., and Ormiston, R., "Tail-Rotor Thrust on a 5.5-Foot Helicopter Model in Ground Effect," American Helicopter Society 30th Annual Forum, Washington, D.C., May 1974.

5. Branum, L. and Chee, T., "Performance and Pressure Data from a Small Model Tilt-Rotor in Hover," NASA TM110441, April 1997.